

15. I. E. T. Iben, in *31st EOS/ESD Symposium* (ESD Association, Rome, NY, 2009), p. 1.
16. X. Chen, A. Hochstrat, P. Borisov, W. Kleemann, *Appl. Phys. Lett.* **89**, 202508 (2006).
17. A. V. Kimel *et al.*, *Nat. Phys.* **5**, 727 (2009).
18. Supporting material is available on Science Online.
19. C. F. Hirjibehedin *et al.*, *Science* **317**, 1199 (2007).
20. C. F. Hirjibehedin, C. P. Lutz, A. J. Heinrich, *Science* **312**, 1021 (2006).
21. O. Waldmann, T. Guidi, S. Carretta, C. Mondelli, A. L. Dearden, *Phys. Rev. Lett.* **91**, 237202 (2003).
22. I. Bose, A. K. Pal, *Eur. Phys. J. B* **77**, 139 (2010).
23. A. A. Khajetoorians, J. Wiebe, B. Chilian, R. Wiesendanger, *Science* **332**, 1062 (2011).
24. P. M. Haney, R. A. Duine, A. S. Núñez, A. H. MacDonald, *J. Magn. Magn. Mater.* **320**, 1300 (2008).
25. S. Urazhdin, N. Anthony, *Phys. Rev. Lett.* **99**, 046602 (2007).
26. S. Loth, M. Etzkorn, C. P. Lutz, D. M. Eigler, A. J. Heinrich, *Science* **329**, 1628 (2010).
27. S. Mørup, D. E. Madsen, C. Frandsen, C. R. H. Bahl, M. F. Hansen, *J. Phys. Condens. Matter* **19**, 213202 (2007).
28. W. Wernsdorfer *et al.*, *Phys. Rev. Lett.* **79**, 4014 (1997).
29. D. Gatteschi, R. Sessoli, J. Villain, *Molecular Nanomagnets* (Oxford Univ. Press, New York, 2006).
30. B. Barbara, E. M. Chudnovsky, *Phys. Lett. A* **145**, 205 (1990).
31. E. E. Fullerton *et al.*, *Appl. Phys. Lett.* **77**, 3806 (2000).

**Acknowledgments:** We acknowledge B. Melior for expert technical assistance. S.L., C.P.L., and A.J.H. thank the Office of Naval Research for financial support. A patent application regarding information storage in antiferromagnetic nanostructures was filed with the U.S. Patent and Trademark Office.

#### Supporting Online Material

www.sciencemag.org/cgi/content/full/335/6065/196/DC1  
Materials and Methods  
Figs. S1 to S7  
Table S1  
References (32–38)

19 September 2011; accepted 28 November 2011  
10.1126/science.1214131

# Composites Reinforced in Three Dimensions by Using Low Magnetic Fields

Randall M. Erb, Rafael Libanori, Nuria Rothfuchs, André R. Studart\*

The orientation and distribution of reinforcing particles in artificial composites are key to enable effective reinforcement of the material in mechanically loaded directions, but remain poor if compared to the distinctive architectures present in natural structural composites such as teeth, bone, and seashells. We show that micrometer-sized reinforcing particles coated with minimal concentrations of superparamagnetic nanoparticles (0.01 to 1 volume percent) can be controlled by using ultralow magnetic fields (1 to 10 milliteslas) to produce synthetic composites with tuned three-dimensional orientation and distribution of reinforcements. A variety of structures can be achieved with this simple method, leading to composites with tailored local reinforcement, wear resistance, and shape memory effects.

The widespread use and increasing relevance of composite materials are primarily due to their higher strength-to-weight ratio (specific strength) compared to metals, and higher toughness (flaw tolerance) compared to ceramics. Polymer-matrix composites are predominantly assembled with ceramic, metal, or polymeric one-dimensional (1D) reinforcement such as glass, steel, aramide (Kevlar), or carbon long fibers. These fibers are typically tens of micrometers in diameter and increase the strength and stiffness along the long axis of the reinforcement because of the transfer of stress across the reinforcement-polymer interfaces parallel with the load. (1) However, 1D reinforcement makes manufactured materials weak in the other two dimensions, which can be partially overcome through laminating 1D layers at varied angles, weaving fibers into 2D arrays, by using 2D reinforcement particles such as platelets or synthesizing lamellar structures (1–9).

Few 3D reinforcement solutions have been proposed to reinforce artificial composites, including the insertion of out-of-plane fibers by mechanical punching (10); the formation of special fiber arrays by using textile processes like

weaving, braiding, stitching, and knitting (11); and the growth of aligned carbon nanotubes on the surface of the reinforcing woven fibers (12, 13). Three-dimensional reinforcement is also present in composites containing randomly oriented short fibers or platelets. However, these approaches either lead to a decrease in in-plane mechanical properties or do not allow for deliberate control over the distribution and 3D orientation of high concentrations of reinforcing nano- and micro-particles. The lack of controlled reinforcement in the third dimension makes manufactured composites susceptible to impact damage (2, 14), wear (15), longitudinal microbuckling of fibers (16), delamination (2), and long-term fatigue (13, 17).

Structural biological composites tackle this problem by accurately controlling the orientation of anisotropic nano- and micro-sized building blocks so as to reinforce the material in specific directions to multidirectional external loads (18–20). Examples include the spiral twisting of mineralized collagen fibrils in bone (21); the out-of-plane oriented calcite prisms and in-plane oriented aragonite platelets in the outer and inner layers of seashells, respectively (22); and the out-of-plane oriented hydroxyapatite prisms and in-plane oriented mineralized collagen fibrils in tooth enamel and dentin, respectively (23). Capturing some of the design principles underlying the exquisite architecture of such biological materials would allow us to overcome many of

the mechanical limitations of current artificial composites.

We propose a strategy to obtain microstructured artificial composites exhibiting 3D architectures and enhanced mechanical behavior. The approach relies on the application of external magnetic fields and field gradients to align and position anisotropic reinforcing microparticles within the composite matrix. As typical reinforcing particles are often diamagnetic, requiring extremely high magnetic fields for alignment (~1 T) (24), we first coat them with superparamagnetic nanoparticles to make them more responsive to magnetic fields. Though a similar method has been previously used (25) to align carbon nanotubes with fields in the range 0.2 to 1 T, we have discovered through experiments and theoretical energy models that using the right geometry of reinforcement particles leads to an ultrahigh magnetic response (UHMR). Indeed, the magnetic field required to align the reinforcement particles can be reduced to the value of 0.8 mT. This alignment field is only an order of magnitude above Earth's natural magnetic field (~0.05 mT) and is orders of magnitude below the magnetic field of rare-earth magnets (~200 mT), common solenoids (~20 mT), and even standard refrigerator magnets (~10 mT).

To determine the optimum particle size that will show an UHMR effect, we theoretically predict the minimum magnetic field required for alignment,  $H_{\min}$ , for different sizes, aspect ratios, and geometries of reinforcing elements. The dependence of  $H_{\min}$  on the size of nonmagnetic platelets and rods coated with magnetic material can be estimated by computing the difference in magnetic ( $U_m$ ) and gravitational ( $U_g$ ) energies of the system as compared to the internal thermal energy ( $k_B T$ , where  $k_B$  is the Boltzmann factor and  $T$  is temperature) that serves to randomize alignment. The magnetic energy  $U_m$  is calculated with an ellipsoidal shell model that reflects that the slight amount of magnetic material lies only in an outer layer coating the reinforcing element (SOM text). The magnetic energy is dependent upon the particle's orientation with respect to the magnetic field,  $\psi$ , and is smallest when the long axis of the particle is parallel with the applied magnetic field ( $\psi = 0^\circ$ ). Further, the gravitational energy of a particle resting on a horizontal surface is also dependent upon the orientation with

Complex Materials, Department of Materials, ETH Zurich, 8093 Zurich, Switzerland.

\*To whom correspondence should be addressed. E-mail: andre.studart@mat.ethz.ch

respect to the surface,  $\theta$ , and is smallest when the particle's long axis is parallel with the surface ( $\theta = 0^\circ$ ).

To estimate the minimum magnetic field required for alignment, we describe the system in terms of a canonical partition function  $Z$ , with the out-of-plane alignment as one of the possible energy states. We consider the case of out-of-plane magnetic fields, for which  $\psi = 90^\circ - \theta$ . The effect of the particle characteristics on  $H_{\min}$  is investigated by computing the magnetic field strength that ensures that most UHMR particles in suspension exhibit a reasonably good alignment—i.e., angles within the range  $75^\circ$  to  $90^\circ$ . The probability  $P_{75^\circ-90^\circ}$  that 90% of the UHMR particles are within this range can be determined by dividing the Boltzmann factor of this out-of-plane state by the partition function as follows:

$$P_{75^\circ-90^\circ} = \int_{75^\circ}^{90^\circ} e^{[U_m(H_{\min}, \psi) - U_g(\theta)]/k_B T} d\theta / Z = 0.9$$

where  $Z = \int_0^{90^\circ} e^{[U_m(H_{\min}, \psi) - U_g(\theta)]/k_B T} d\theta$  (1)

Here,  $Z$  is the sum of the Boltzmann factors of all possible states of orientation of the particles. The equations used to calculate the potential energies  $U_m$  and  $U_g$  are available online (SOM text). To simplify the analysis and obtain a first approximation for  $H_{\min}$ , we neglect the contributions of orientational and packing entropy to the free energy of the system (26). This simplification is partly justified in that packing entropy is only relevant for particle concentrations higher than those used in most of our experiments (14.2 vol % platelets, SOM text).

Our model predictions indicate that the alignment of nonmagnetic platelets and rods of 5 and 10  $\mu\text{m}$  in length, respectively, with modest surface coatings of iron oxide nanoparticles ( $\sim 0.5$  vol %) requires fields that are orders of magnitude lower than for particles with different geometries (Fig. 1, A and C). Thermal and gravitational energies dominate for particles smaller and larger than a few micrometers, respectively, which substantially increases the field required for alignment.

To verify the theoretical analysis, we apply magnetic fields to surface-magnetized platelets and rods with average size within the optimum range required for alignment. The magnetized surface coating is formed upon addition of the reinforcing particles to an aqueous suspension of 12-nm iron oxide nanoparticles with oppositely charged surface at a specific pH. Under these conditions, adsorption is driven through electrostatic interactions and is further enhanced by short-range van der Waals attraction, eventually becoming irreversible. We investigate both 7.5- $\mu\text{m}$ -long, 200-nm-thick alumina platelets (Alusion, Antaria, Bentley, Australia) and 10- $\mu\text{m}$ -long, 1- $\mu\text{m}$ -thick calcium sulfate hemihydrate rods that exhibit, respectively, positive and negative surface charge in water at pH = 7 (27). To coat such reinforcing elements, we add 1 vol % particles (platelets or rods) in aqueous suspensions of 0.0052

vol % oppositely charged iron oxide nanoparticle suspensions (anionic EMG-705 or cationic EMG-605, Ferrotec, Germany) until complete adsorption occurs (Fig. 1E).

The magnetic field required to align the surface-magnetized platelets and rods agrees very well with the theoretical estimates (Fig. 1, B and D, and movie S1), confirming that it is possible to orient reinforcing elements of a few micrometers in length by using very low magnetic fields. Changing the initial concentration of iron oxide nanoparticles in the suspension controls the magnetization of the reinforcing particles. We have found that the selection of anisotropic particles within the optimum size range enables minimum use of the iron oxide nanoparticles, down to even a few hundred parts per million (0.01 vol %) of magnetic particles with respect to the reinforcing element. Such a concentration of magnetic particles requires a field of 30 mT (Fig. 1F).

This UHMR effect is favored by the 2D confinement of magnetic nanoparticles on the sur-

face of the reinforcing particles. The field required for alignment of the hypothetical case in which magnetic particles are homogeneously distributed throughout the entire volume of the reinforcing element is 69% larger than if the magnetic nanoparticles are only on the surface (SOM text). The confinement of magnetic nanoparticles to increase the magnetic response of anisotropic objects is in fact also used by magnetotactic bacteria to align themselves along Earth's magnetic field to find regions in the ocean with low oxygen concentrations (28).

The ultrahigh magnetic response of the coated anisotropic particles is of general interest in applications that require combined spatial and orientational control of suspended particles (29). We exploit this effect to orient reinforcing particles in a polymer matrix and thus obtain artificial composites exhibiting distinctive mechanical reinforcing and shape memory effects.

Reinforced composites with controlled orientation of reinforcements are prepared by dispersing

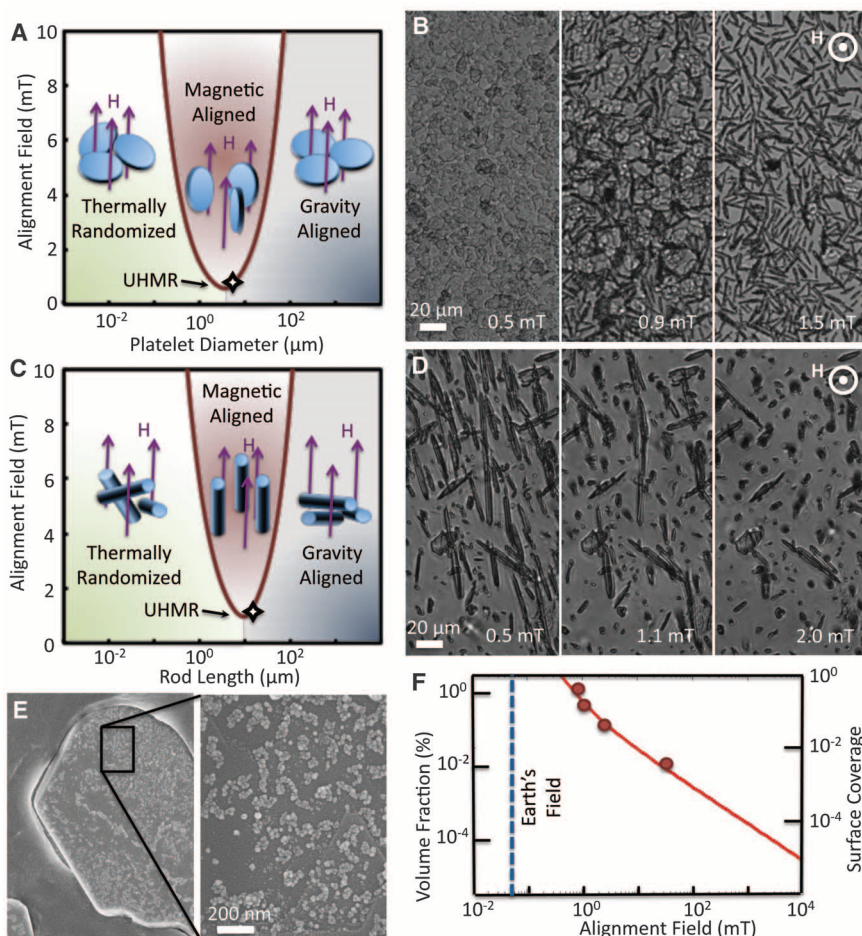


**Fig. 1.** Ultrahigh magnetic response (UHMR) of surface-magnetized rods and platelets. The theoretical minimum alignment field,  $H_{\min}$ , is plotted for (A) platelets (aspect ratio,  $s = 37$ ) and (C) rods ( $s = 30$ ) with a surface coating of magnetic nanoparticles of 0.5 vol %. Specific gravity values of 3.98 and 2.5  $\text{g}/\text{cm}^3$  were used in the calculations, consistent with the experimentally studied alumina platelets and calcium sulfate rods, respectively. Iron oxide-coated (B) alumina platelets and (D) calcium sulfate hemihydrate rods with optimum sizes exhibit an ultrahigh magnetic response, aligning with the extremely low magnetic fields predicted by the theory. (E) Example of 0.5 vol % (13% surface coverage) of iron oxide nanoparticles on an alumina platelet that leads to alignment at 1 mT consistent with theory in (F).

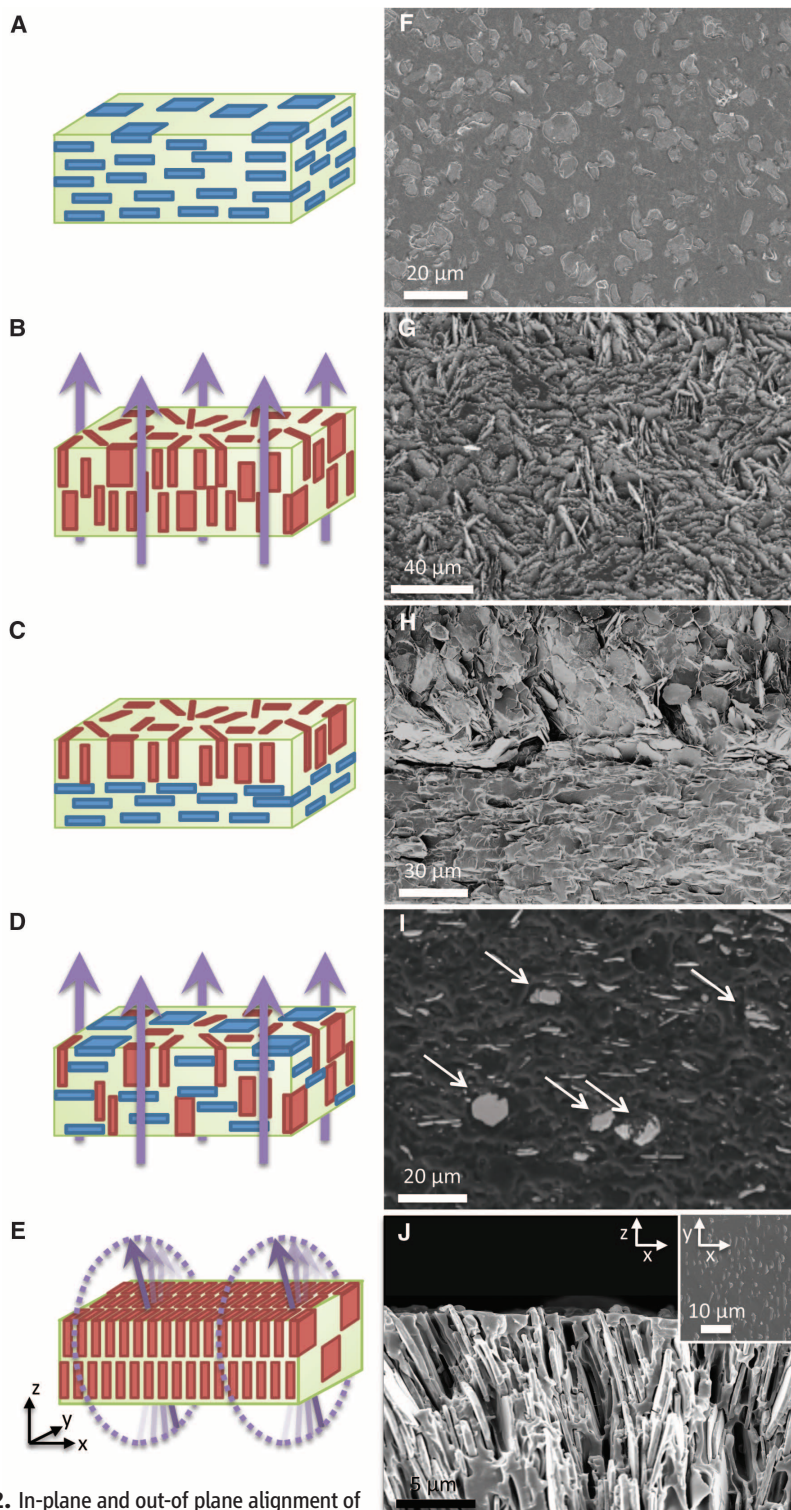


**Fig. 2.** In-plane and out-of plane alignment of UHMR alumina platelets in polyurethane-based composites. (A and B) Schematic and (F and G) top-view scanning electron micrographs (SEMs) of in-plane and out-of-plane reinforced composites (20 vol %  $\text{Al}_2\text{O}_3$  in polyurethane), made without and with an out-of-plane magnetic field, respectively. (C) Schematic and (H) SEM of cross section of laminated layers of in- and out-of-plane reinforced composites (20 vol %  $\text{Al}_2\text{O}_3$  in polyurethane). (D) Schematic and (I) SEM of cross section of mixed alignment with 5 vol % highly magnetized (1 wt %  $\text{Fe}_3\text{O}_4/\text{Al}_2\text{O}_3$ ) and 5 vol % weakly magnetized (0.1 wt %  $\text{Fe}_3\text{O}_4/\text{Al}_2\text{O}_3$ ) alumina platelets in polyurethane produced with sequential magnetic field applications. Arrows indicate platelets in the second orientation direction. (E) Schematic and (J) SEM of cross section of an alumina-polyurethane composite formed under rotating magnetic field that allows for ultrahigh packing fractions. Inset shows top view of composite.

UHMR anisotropic particles in a fluid, aligning and positioning them with a magnetic field, and finally consolidating the fluid to fix the oriented structure. Consolidation may occur through solvent evaporation if the fluid is a polymer solution, through temperature- or light-induced reactions if the fluid is a monomeric solution, or by simply cooling a molten polymeric matrix. We find that the higher viscosity of some of the polymer solutions and resins used for composite fabrication slows the orientation process but does not change the minimum magnetic field required for alignment.

Examples of composites obtained by applying linear, uniform magnetic fields to fluid suspensions containing magnetite-coated alumina platelets, thermoplastic polyurethane elastomer (PU, Elastollan C 64 D 53, BASF), and polyvinylpyrrolidone (PVP, Sigma-Aldrich, molecular mass 360,000 g/mol) are shown in Fig. 2, A, B, F, and G. In these examples, 2.4 g of platelets, 2.2 g of polyurethane, and 0.75 g of polyvinylpyrrolidone were suspended or dissolved in 150 ml of dimethylformamide (DMF, Sigma-Aldrich), and the end composites contained 60 vol % PU, 20 vol % PVP, and 20 vol % alumina. The orientation of the UHMR particles in the consolidated matrices directly reflects the direction of the magnetic field applied. Magnetic alignment and fixation of the UHMR platelets were also possible by using epoxy and acrylate-based resins as polymeric matrix.

In addition to homogeneously reinforced polymers, multilayer composites are easily obtained by laminating together layers of reinforced polymer with specific orientations (Fig. 2, C and H). The resulting composites exhibit an external layer with out-of-plane oriented platelets and an internal layer with in-plane oriented platelets. This should lead to a highly structured artificial composite displaying the unusual and often-desired combination of hardness and wear resistance in the outer layer and strength and toughness in the inner layer by using the same basic building blocks. Single-batch synthesis composites with this architecture can also be prepared simply by mixing reinforcing particles with different magnetic nanoparticle coverage during processing and then applying a combination of magnetic fields. To demonstrate this, we added 4.025 g each of platelets with 13% and 1% surface coverage of iron oxide to 20 g polyurethane (RoPlasthan 2020R, resin-to-hardener weight ratio 3:1) and poured the mixture into a polyethylene mold. The sample was then subjected to an 80-mT horizontal field for 5 min followed by a 10-mT vertical field for 10 min. The resulting structure shows platelets in both configurations, depending upon their surface coverage (Fig. 2, D and I). Further, because of the low concentration of iron oxide nanoparticles within the composite and the slight permeability of water through the polyurethane matrix, in this system it is even possible to completely remove magnetic iron oxide nanoparticles for applications that forbid even this slight mag-

netic content. This can be accomplished by submerging the consolidated material in a permeating phosphoric acid aqueous solution to completely dissolve the iron oxide nanoparticles without affecting the orientation of reinforcing particles (fig. S3) (27).

Although the alignment of platelets by using linear, static magnetic fields allows for the preparation of composites with unusual structures and properties, the concentration of platelets aligned in the out-of-plane direction is limited to about 20 vol % due to steric hindrance effects resulting from the lack of orientational control over the second axis of platelets. This issue can be circumvented by using rotating, linear magnetic fields. A rotating field in the *Y-Z* plane will align the reinforcement platelets along this plane due to energy considerations, pinning two degrees of orientational freedom (Fig. 2, E and J). This alignment is contingent upon the frequency of the rotating field being high enough to prevent synchronous rolling of misaligned platelets. Through such biaxial alignment of the reinforcement platelets, it is possible to reach very high con-

centrations of out-of-plane aligned platelets, even 50 vol %.

Control of the orientation of reinforcing particles enables tailoring of properties in specific directions. We investigated the effect of the orientation of reinforcing particles on the mechanical behavior of homogeneously reinforced polymers by measuring the tensile mechanical properties of specimens containing reinforcement aligned parallel or perpendicular to the applied load (Fig. 3A). The reinforced sample containing 20 vol % parallel-aligned platelets exhibits on average 63% and 86% higher yield strength as compared to the pure matrix and the perpendicular-aligned platelets, respectively. Likewise, the average elastic modulus of the composites with parallel-oriented platelets was 2.8-fold higher as compared to the pure polyurethane matrix, whereas a moderate increase is observed if compared with composites having perpendicular-aligned platelets (table S1 and SOM text).

We use simple rules of mixtures (5) to obtain a quantitative relation between the aligned architecture and the resulting mechanical properties

of the composites. Assuming pull-out mode of fracture, the yield strength,  $\sigma_c$ , of the composite is given by

$$\sigma_c = \phi_p \frac{\tau_y s}{2} + (1 - \phi_p) \sigma_m \quad (2)$$

where  $\tau_y$  is the shear strength of the lesser of either the polymer matrix or the platelet/polymer interface,  $s$  is the platelet aspect ratio,  $\sigma_m$  is the yield tensile strength of the matrix, and  $\phi_p$  is the volume fraction of platelets. Taking  $\sigma_m = 28.6$  MPa (Fig. 3A), we find that the yield strength of the composite with in-line reinforcement ( $\sigma_c = 46.8$  MPa) can be accurately described by Eq. 2 if the value of  $\tau_y$  is equal to 6.5 MPa. Such  $\tau_y$  is lower than the value of 14.3 MPa expected for the shear strength of the polymer matrix ( $\sigma_m/2$ ), suggesting that fracture in this case is controlled by the weaker platelet/polymer interface. This indicates that further reinforcement with parallel-aligned platelets is possible by optimizing the platelet/polymer interfacial bonding in this system.

In addition to the tensile properties, hardness values were measured for homogeneous composites

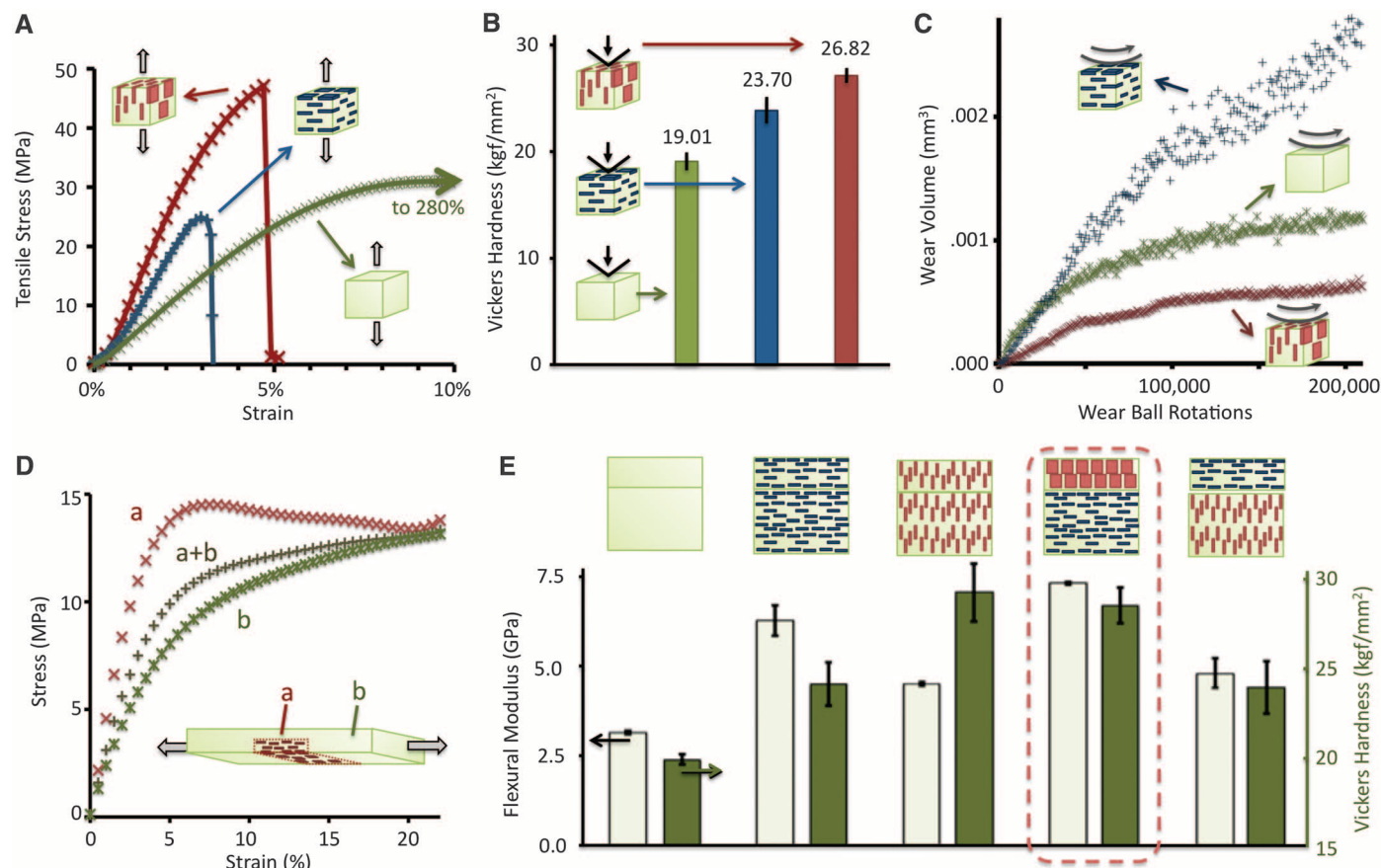


**Fig. 3.** Enhanced mechanical properties of composites containing aligned UHMR platelets. **(A)** Representative increased tensile strength for polyurethane-based polymers with 20 vol %  $\text{Al}_2\text{O}_3$  platelets parallel with applied force (red) versus perpendicular (blue) and nonreinforced (green) samples. **(B)** Increased hardness for reinforced methacrylate resins with 10 vol %  $\text{Al}_2\text{O}_3$  platelets parallel to the applied load versus perpendicular and nonreinforced samples. **(C)** Increased wear resistance for acrylic-based composite films of dental resins with 1 vol % added out-of-plane aligned  $\text{Al}_2\text{O}_3$  reinforcement. **(D)**

Localized stiffening in a polyurethane film by using magnetically induced spatial gradients in the 3 vol %  $\text{Al}_2\text{O}_3$  particle reinforcement. **(E)** Flexural modulus and out-of-plane hardness of bilayer rectangular bars (30 mm by 5 mm by 3 mm) with different combinations of reinforcement orientation. The schematic drawings show the cross sections of the tested structures, with the bottom layer corresponding to the region subjected to tension in three-point bending and the top layer corresponding to the region subjected to out-of-plane hardness measurements.

with 10 vol % UHMR platelets in methacrylate-based composites. Samples with reinforcement particles oriented parallel to the applied load showed increased hardness compared to perpendicular reinforcement and nonreinforced samples (Fig. 3B). Composite films containing alumina platelets aligned out-of-plane also exhibit outstanding wear resistance. Wear was measured by sliding a zirconia ball subjected to a normal load of 1.98 N over acrylate-based composite films with double deionized water as lubricating medium (27). A commercial acrylate-based composite dental resin (Clearfil AP-X, Kuraray, Japan) with 85 wt % isotropic glass microparticles was subjected to wear testing (Fig. 3C) and demonstrated a total wear volume of 0.001 mm<sup>3</sup>. Instead, a nominal 1 vol% of UHMR platelets were added to the resin in both the in-plane and out-of-plane orientations. Orientation of only 1 vol % platelets normal to the wear ball (out-of-plane) decreases the maximum wear volume by 77% as compared

to the samples with in-plane oriented reinforcement. Such wear volume is also 45% lower than that observed in the pure commercial resin. Observation of the worn area of tested films suggests that the out-of-plane oriented hard platelets remain strongly locked within the surrounding polymer matrix, effectively impeding the penetration of the zirconia ball into the material during sliding. In contrast, isotropic particles and in-plane aligned platelets can be more easily removed from the matrix by the shear stresses developed under the sliding ball, leading to more pronounced wear. In contrast to the tensile mechanical properties, a quantitative analysis of the effect of reinforcement orientation on the hardness and wear of such anisotropic structures is less straightforward due to the complicated stress states in these cases.

To illustrate the benefit of building composites with controlled 3D reinforcement, we produced bilayer structures with tailored reinforcement architectures by laminating together layers of 10

vol % alumina platelets in an epoxy resin (similar to those in Fig. 2C) (27). The platelets in each individual layer were aligned both in-plane or out-of-plane by using rotating linear magnetic fields, leading to the structures schematically shown in Fig. 3E. Rectangular bars of the various created structures were evaluated with regards to out-of-plane hardness and flexure modulus under three-point bending. Typically, structures containing platelets aligned in-plane exhibit high flexural modulus but low out-of-plane hardness. Conversely, composites containing only out-of-plane oriented platelets exhibit higher out-of-plane hardness but lower flexural modulus. Instead, by creating a laminate structure exhibiting out-of-plane alignment in the upper layer and in-plane orientation in the bottom layer, one can produce a composite with both increased flexural modulus and increased out-of-plane hardness. Despite the much lower concentration of inorganic phase present in the synthetic composites, a similar architecture is found in seashells (22).

Exploiting various conventional magnetophoretic techniques with these UHMR reinforcement particles allows for the facile synthesis of even more elaborate composite architectures. For example, this technique can be used to concentrate UHMR particles to specific regions of the film before consolidation of the matrix. In this case, a magnetic field gradient has to be established to drive the UHMR particles to the region of interest. This is exemplified in Fig. 4, A and D, by a polyurethane/alumina composite exhibiting out-of-plane aligned UHMR platelets that were concentrated on the surface of the film. To demonstrate that concentrated UHMR particles can locally reinforce the polymer matrix, we conducted tensile tests on 2 mm by 12 mm by 0.1 mm polyurethane samples with a 5-mm stripe of reinforced area produced with a hand-held rare-earth magnet (Fig. 3D). The highly heterogeneous composite obtained exhibit distinct local elastic moduli that can be estimated by using simple rules of mixtures (SOM text). Local stiffening of 180% was estimated by evaluating the elastic modulus of the reinforced and nonreinforced areas in independent tensile tests (Fig. 3D, SOM text). A straightforward extension of this method is to use spatial magnetic gradients to locally reinforce around weak points of a composite part, as exemplified in Fig. 4, B and E, for a composite with 5 vol % UHMR particles in poly(vinyl alcohol) containing a central hole (PVA, molecular mass = 13,000 to 23,000 g/mol, Sigma Aldrich).

The possible reinforcement orientations that can be achieved are in principle only limited by the magnetic field patterns that can be created. Indeed, ordinary refrigerator magnets that exhibit multiple magnetic domain patterns can be used to produce composites with reinforcing particles that gradually change orientation across the film (Fig. 4, C and G). Such tailored local orientation of reinforcing elements is a key design principle to control organ movements in wood cells and wheat awns (30). The physical constraints im-

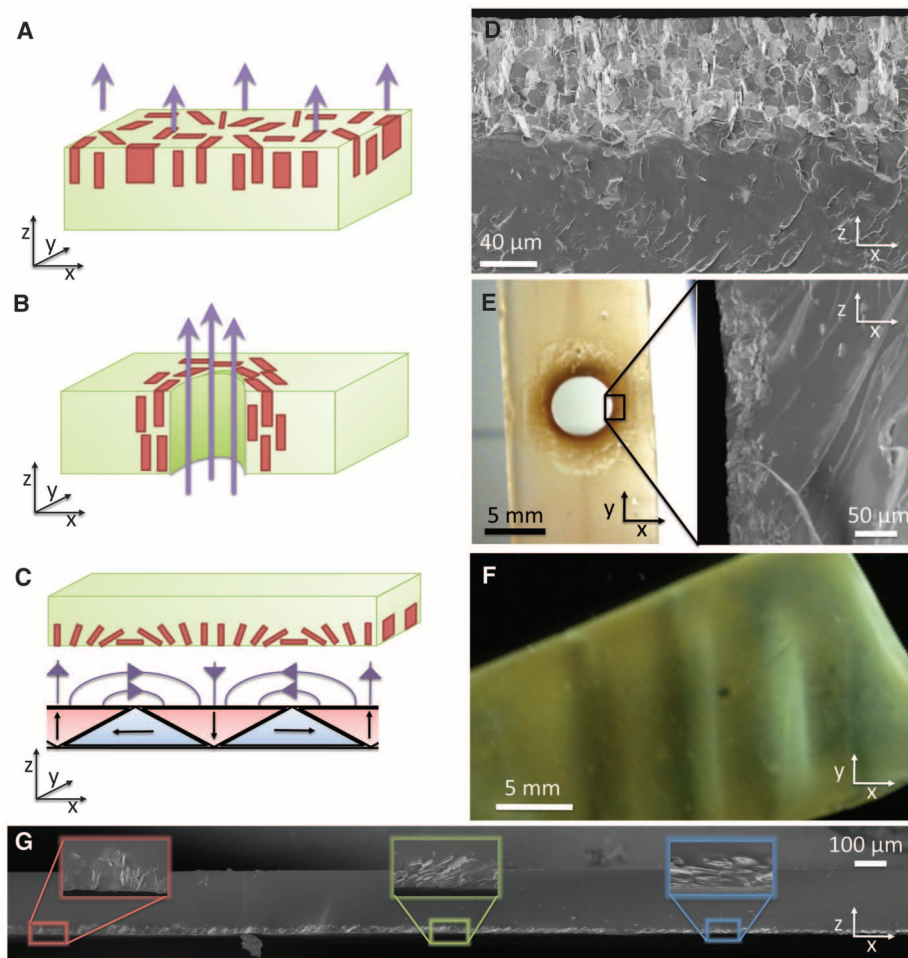


**Fig. 4.** Unusual 3D reinforcement architectures through advanced orientational and spatial magnetic control. (A and B) Schematic and (D and E) SEMs of cross-section of a spatial gradient in UHMR particles attracted preferentially to the composite edge or around a material weak point, respectively, due to a magnetic field gradient. Composites are 5 vol % Al<sub>2</sub>O<sub>3</sub> in (D) polyurethane and (E) PVA. (C) Schematic of a standard refrigerator magnet's domain structure leading to gradually varying UHMR particle alignment as seen in (G) for a 5 vol % Al<sub>2</sub>O<sub>3</sub> in PVA swellable composite. Such structures can locally swell to different extents depending on the platelet orientation, leading to the reversible formation of topographical ripples in the polymer (F).

posed by the cellulose microfibrils specially arranged on the plant cell wall lead to complex actuation behavior. Likewise, we demonstrate that PVA hydrogel films containing reinforcing platelets with gradually changing local orientation can reversibly change their shape from straight to well-defined wavy patterns upon drying or swelling of the hydrogel matrix (Fig. 4F).

Given the possibility to precisely control the position and orientation of reinforcing particles within the matrix, the method outlined here offers a way to locally tailor the properties of composite materials by using the same set of initial building blocks. The myriad of unusual properties including out-of-plane global or local increases in composite stiffness, strength, hardness, wear resistance, and the shape memory effect achieved by simply controlling the orientation and position of reinforcing elements suggest the enormous potential of this approach.

#### References and Notes

1. D. Hull, T. W. Clyne, *An Introduction to Composite Materials*, D. R. Clarke, S. Suresh, I. M. Ward, Eds., Cambridge Solid State Science Series (Cambridge Univ. Press, Cambridge, 1996).
2. T. W. Chou, *Microstructural Design of Fiber Composites* (Cambridge Univ. Press, Cambridge, 1992).
3. E. Munch *et al.*, *Science* **322**, 1516 (2008).

4. S. Deville, E. Saiz, R. K. Nalla, A. P. Tomsia, *Science* **311**, 515 (2006).
5. L. J. Bonderer, A. R. Studart, L. J. Gauckler, *Science* **319**, 1069 (2008).
6. Z. Y. Tang, N. A. Kotov, S. Magonov, B. Ozturk, *Nat. Mater.* **2**, 413 (2003).
7. A. Walther *et al.*, *Nano Lett.* **10**, 2742 (2010).
8. P. Podsiadlo *et al.*, *Science* **318**, 80 (2007).
9. Z. Burghard *et al.*, *Nano Lett.* **9**, 4103 (2009).
10. G. Freitas, C. Magee, P. Dardzinski, T. Fusco, *J. Adv. Mater.* **25**, 36 (1994).
11. A. P. Mouritz, M. K. Bannister, P. J. Falzon, K. H. Leong, *Compos. Part A Appl. Sci. Manuf.* **30**, 1445 (1999).
12. V. P. Veedu *et al.*, *Nat. Mater.* **5**, 457 (2006).
13. H. Qian, E. S. Greenhalgh, M. S. P. Shaffer, A. Bismarck, *J. Mater. Chem.* **20**, 4751 (2010).
14. W. J. Cantwell, J. Morton, *Composites* **22**, 347 (1991).
15. S. Ozcan, P. Filip, *Wear* **259**, 642 (2005).
16. P. M. Jelf, N. A. Fleck, *J. Compos. Mater.* **26**, 2706 (1992).
17. L. Tong, A. P. Mouritz, M. Bannister, *3D Fibre Reinforced Polymer Composites* (Elsevier, Amsterdam, 2002).
18. C. Ortiz, M. C. Boyce, *Science* **319**, 1053 (2008).
19. P. Fratzl, R. Weinkamer, *Prog. Mater. Sci.* **52**, 1263 (2007).
20. F. Barthelat, C. M. Li, C. Comi, H. D. Espinosa, *J. Mater. Res.* **21**, 1977 (2006).
21. W. Wagermaier *et al.*, *Biointerphases* **1**, 1 (2006).
22. H. J. Qi, B. J. F. Bruet, J. S. Palmer, C. Ortiz, M. C. Boyce, in *Mechanics of Biological Tissues*, G. A. Holzapfel, R. W. Ogden, Eds. (Springer-Verlag, Graz, Austria, 2005).
23. V. Imbeni, J. J. Kruzic, G. W. Marshall, S. J. Marshall, R. O. Ritchie, *Nat. Mater.* **4**, 229 (2005).
24. D. van der Beek *et al.*, *Phys. Rev. E* **73**, 011409 (2006).
25. M. A. Correa-Duarte *et al.*, *J. Phys. Chem. B* **109**, 19060 (2005).

26. L. Onsager, *Ann. N.Y. Acad. Sci.* **51**, 627 (1949).
27. Materials and methods are available as supporting material on Science Online.
28. D. Fèvre, D. Schüller, *Chem. Rev.* **108**, 4875 (2008).
29. S. B. Bubenhofner *et al.*, *Nanotechnology* **20**, 485302 (2009).
30. P. Fratzl, R. Elbaum, I. Burgert, *Faraday Discuss.* **139**, 275, discussion 309, 419 (2008).

**Acknowledgments:** We thank T. Tervoort, L. van Breemen, K. Feldman, M. Imhof, J. Hofstetter, R. Stahel, R. Ehrbar, P. Zweifel, B. Wegmann, and M. Schinhammer for experimental assistance, and Antaria, Huntsman Advanced Materials, Rosen and BASF for supplying the alumina platelets, polymers, and resins. We acknowledge internal funding from ETH Zurich and the Swiss National Science Foundation (grant 200021\_135306/1), as well as support by the Electron Microscopy Center of ETH Zurich (EMEZ). ETH Zurich has applied for the following patent: A. R. Studart, R. M. Erb, R. Libanori, Method for the production of reinforced materials and reinforced materials obtained using the method, European patent application 10003358.8, priority date 29 March 2010.

#### Supporting Online Material

[www.sciencemag.org/cgi/content/full/335/6065/199/DC1](http://www.sciencemag.org/cgi/content/full/335/6065/199/DC1)  
Materials and Methods  
SOM Text  
Figs. S1 to S11  
References (31–40)  
Movie S1  
7 July 2011; accepted 25 October 2011  
10.1126/science.1210822

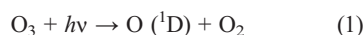
## Direct Kinetic Measurements of Criegee Intermediate (CH<sub>2</sub>OO) Formed by Reaction of CH<sub>2</sub>I with O<sub>2</sub>

Oliver Welz,<sup>1</sup> John D. Savee,<sup>1</sup> David L. Osborn,<sup>1</sup> Subith S. Vasu,<sup>1</sup> Carl J. Percival,<sup>2</sup> Dudley E. Shallcross,<sup>3</sup> Craig A. Taatjes<sup>1\*</sup>

Ozonolysis is a major tropospheric removal mechanism for unsaturated hydrocarbons and proceeds via “Criegee intermediates”—carbonyl oxides—that play a key role in tropospheric oxidation models. However, until recently no gas-phase Criegee intermediate had been observed, and indirect determinations of their reaction kinetics gave derived rate coefficients spanning orders of magnitude. Here, we report direct photoionization mass spectrometric detection of formaldehyde oxide (CH<sub>2</sub>OO) as a product of the reaction of CH<sub>2</sub>I with O<sub>2</sub>. This reaction enabled direct laboratory determinations of CH<sub>2</sub>OO kinetics. Upper limits were extracted for reaction rate coefficients with NO and H<sub>2</sub>O. The CH<sub>2</sub>OO reactions with SO<sub>2</sub> and NO<sub>2</sub> proved unexpectedly rapid and imply a substantially greater role of carbonyl oxides in models of tropospheric sulfate and nitrate chemistry than previously assumed.

In 1949, Rudolf Criegee proposed that ozonolysis of alkenes proceeds via carbonyl oxide biradicals, in an ozonolysis mechanism that is now generally accepted (1). Because a large fraction of the tropospheric oxidation of unsaturated hydrocarbons is initiated by reaction

with ozone (2), these biradical “Criegee intermediates” play a substantial role in the tropospheric budgets of secondary organic aerosols (SOAs), ozone, NO<sub>x</sub>, NO<sub>y</sub>, and HO<sub>x</sub>. For example, the OH radical, key to the oxidizing capacity of the troposphere, is formed by a sequence of photochemical reactions involving ozone:



These reactions depend on the presence of sunlight and water vapor. However, field mea-

surements (3) have shown that OH levels in winter and summer are very similar in UK urban environments (4), despite the fact that in winter the efficiency of the reaction in Eq. 1 drops by at least 50%. Harrison *et al.* (4) showed that winter production of OH via ozonolysis of alkenes, dominated by Criegee radical chemistry, makes up this difference. SOAs can also be initiated by Criegee intermediate reactions (5, 6).

Although decades of theoretical studies and indirect experimental evidence support the importance of Criegee radicals in the troposphere [e.g., (7)], the quantitative effects of their chemistry remain uncertain (8) because it has been impossible to make direct measurements of Criegee reactions with key atmospheric species. Until now, determination of rate constants for Criegee reactions has been carried out by investigating changes in the products of ozonolysis upon addition of different reagents or scavengers (9, 10). Interpretation of such experiments requires modeling the full complexity of ozonolysis, in which the production, stabilization, and removal of Criegee intermediates are all imperfectly understood. Although an internally consistent picture of Criegee chemistry has been slowly emerging (11), absolute rate coefficient estimates with key atmospheric species continue to range over 4 to 5 orders of magnitude (12).

Recently the photoionization spectrum of the simplest gas-phase Criegee intermediate, formaldehyde oxide (which we denote as CH<sub>2</sub>OO), was measured in the chlorine atom-initiated oxidation of dimethyl sulfoxide (DMSO) (13). In

<sup>1</sup>Combustion Research Facility, Mail Stop 9055, Sandia National Laboratories, Livermore, CA 94551-0969, USA. <sup>2</sup>School of Earth, Atmospheric and Environmental Sciences, University of Manchester, Williamson Building, Oxford Road, Manchester M13 9PL, UK. <sup>3</sup>School of Chemistry, University of Bristol, Bristol BS8 1TS, UK.

\*To whom correspondence should be addressed. E-mail: cataatj@sandia.gov